

3D VSP processing and imaging: A case study at Mad Dog, Gulf of Mexico

Chang-Chun Lee*, Weiping Gou, CGG

Francis Rollins, Qingsong Li, Tianxia Jia, Samarjit Chakraborty, BP

Summary

3D VSP data provides a unique opportunity to improve image resolution and fault definition in the vicinity of a well. However, the processing and imaging of VSP data requires special accommodations for its distinctive acquisition geometry. In this abstract, we demonstrate two key VSP pre-processing steps that greatly impacted the final image from the Mad Dog 3D VSP data, including XYZ vector field reorientation based on 3D elastic finite-difference modelling, and shot-to-shot directional designation using near field hydrophone data. We also discuss how utilizing the multiple energy - in addition to primary - extends our capability to image the shallow overburden.

Introduction

The Mad Dog field, one of the giant fields in BP's Gulf of Mexico (GoM) portfolio, was discovered by BP in 1998 and began producing in 2005. The field is located at the edge of the Sigsbee Escarpment, 190 miles south of New Orleans. Like many other subsalt fields in the GoM, seismic imaging at the Mad Dog field is challenging due to the complex salt structure in the overburden (Figure 1). Great efforts have been made to obtain a better tilted transverse isotropic (TTI) velocity model for the Mad Dog field using multi-wide azimuth data (Rollins et al., 2013). Yet 3D VSP surveys may offer even better opportunities to obtain high quality imaging near the wellbore compared to surface steamer data due to less distorted wave propagation paths (Rollins et al., 2015). To assist the continued development of the Mad Dog field in the GoM, BP acquired the largest conventional 3D VSP data set to date in the world in July 2015, intending to complement the existing towed steamer data. The Mad Dog VSP survey featured a shot coverage diameter of approximately 50,000 ft at the surface and 100 receivers placed down the well at a 65.6-foot interval, down to 22,000 ft. Each receiver consisted of three individual geophones, XYZ components, mounted orthogonally to each other.

To produce an image truly complementary to existing steamer data, several VSP imaging challenges must be addressed, beginning with preparations to ensure constructive stacking among all the downhole receivers. After placement downhole, the orientation of each receiver is unknown; thus, aligning all the receivers to the same orientation (Cardinal directions and true vertical) is critical. Incorporating auxiliary instruments like gyroscopes or inclinometers in the downhole can give some indication of

local attitude relative to an external reference field. However, small gyroscopes often drift from their original positions, and inclinometers may increase the cost and weight of downhole receivers (Greenhalgh et al., 1995). For these reasons, no auxiliary instruments were installed in the Mad Dog 3D VSP survey, and an alternative approach to determine the orientation of triaxial geophone was required. By comparing the geophone response to a known elastic wavefield, we applied an algorithm using 3D TTI elastic modeled synthetic data to calibrate the orientation for each receiver (Dy, personal communication, 2015).

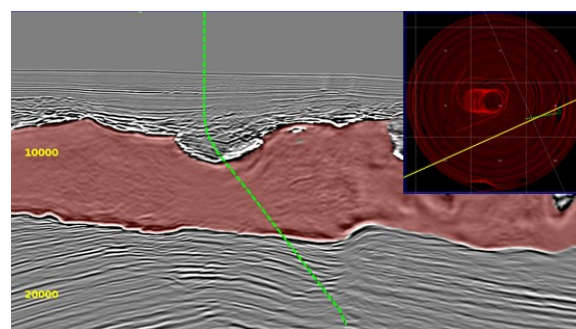


Figure 1: A section view showing the challenges of the Mad Dog field due to complex salt geometry. Well trajectory is indicated by the green dash line. The inset shows the shot location (red) and well trajectory (green).

As it is for surface steamer data, also important for imaging VSP data is the removal of the bubble energy and source signature. In surface steamer acquisition, this is often done by using the far-field source wavelet to remove the source signature and bubble energy (i.e., 1D designation), which is a close approximation for data with limited offset and azimuth ranges. However, due to the Mad Dog 3D VSP survey's long-offset and full-azimuth acquisition geometry, the 1D designation method was not sufficient. We utilized near field hydrophone (NFH) data to perform shot-to-shot directional designation (Lee et al., 2014; Li et al., 2015) on the 3D VSP data using an inversion algorithm. This process removed the low-frequency bubble energy and the distinct gun signature among different azimuths and take-off angles caused by the spatial extent and the asymmetry of the gun array.

While VSP surveys are acquired primarily for the purpose of providing complementary high resolution images in challenging, local subsurface areas around wellbores, the extent of the imaging area is severely limited by the extent

3D VSP imaging at Mad Dog, Gulf of Mexico

of the up-going energy. However, the free-surface multiple wavefields are also recorded in the VSP data. Though traditionally considered as coherent noise in up-going VSP imaging, multiple energy can illuminate a significantly larger area; if successfully utilized, the multiple energy could extend images further beyond the wellbores. However, migration of multiples is not straightforward. Leung et al. (2013) demonstrated a synthetic example of Reverse Time Migration of Multiples (RTMM) imaging for VSP by separating up- and down-going waves. In the same year, O'Brien et al. also utilized free-surface multiples in walkaway VSP imaging. Employing an algorithm for migration of multiples, we demonstrated the imaging improvement at the Mad Dog field - the area imaged by the migration of multiples was greatly extended, especially in the shallow overburden.

XYZ vector field reorientation

In the Mad Dog VSP survey, each receiver consisted of three individual geophones mounted orthogonally to each other (XYZ). When placed downhole, the X- and Y-orientations were completely unknown, while the Z-orientation was somewhat aligned with the dipping direction at an unknown degree of tilt. To stack the image from all 100 receivers, aligning the XYZ components to the true Cardinal directions and true vertical depth was necessary. We used 3D TTI elastic wave equation modeling to generate XYZ wavefields at the geophone locations. Let \vec{A} be the 3C field data from the real data, \vec{A}' the 3C field data from the modeled data, and \vec{R} be the unknown tilt correction matrix. The following steps were used to reorient receivers (Dy, personal communication, 2015):

1. Pick first arrival energy for the synthetic and real data for each component.
2. Using first arrival energy, estimate the rotation angle that can align the real data with the rotated synthetic data, i.e., find \vec{R} that minimizes $|\vec{A} - \vec{R}^{-1}\vec{A}'|$. This is performed by scanning all possible rotation angles.
3. Apply individual rotation matrix \vec{R} to each receiver.

In this exercise, the process of generating synthetic data is computationally expensive because the 3D TTI elastic modeling must honor the real shot/receiver acquisition geometry and over 12,000 shots are modelled.

The impact of the XYZ vector field reorientation on the time-domain seismic data and migrated image is shown in Figures 2 and 3. The shot gathers are more coherent for all the receivers, especially for the X- and Y- components. We also see significant improvement in the migrated image

after reorientation. To produce a better VSP Z-component imaging from a much deviated well, performing XYZ vector field reorientation before migration is critical.

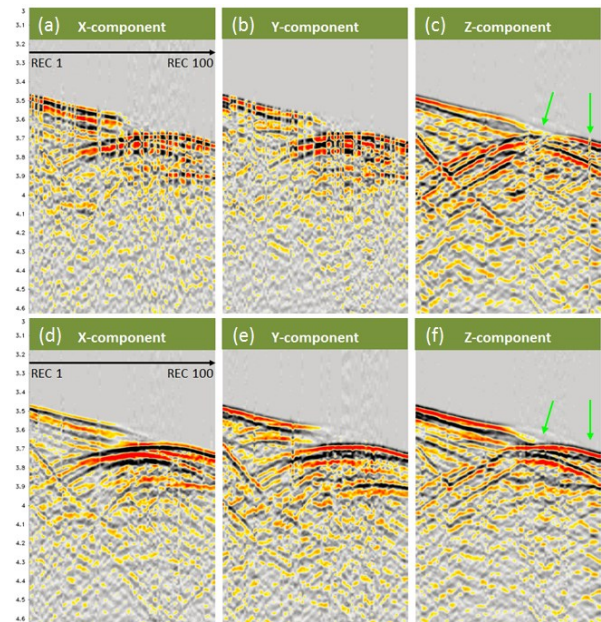


Figure 2: Shot gathers for 100 receivers before XYZ vector field reorientation for (a) X-, (b) Y- and (c) Z-components and after reorientation for (d) X-, (e) Y- and (f) Z-components.

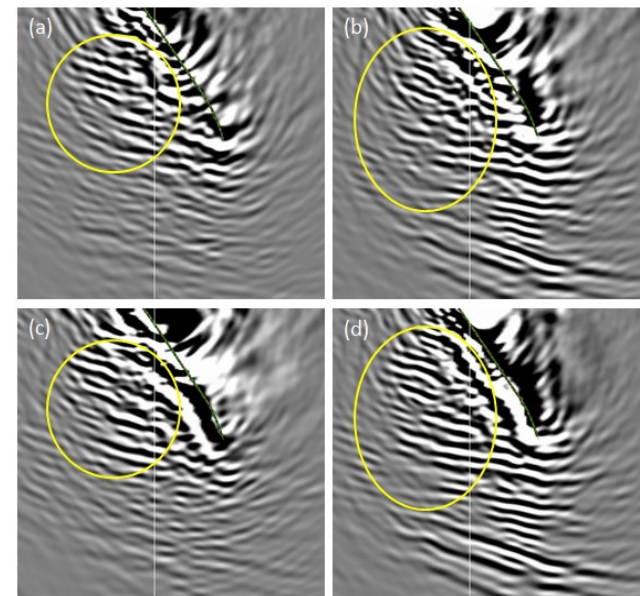


Figure 3: Migrated images before and after XYZ vector field reorientation. (a) Y- and (b) Z-components before reorientation. (c) Y- and (d) Z-components after reorientation.

3D VSP imaging at Mad Dog, Gulf of Mexico

Shot-to-shot directional designature

In marine acquisition, the energy source consists of several air guns in an array. Each gun has its own characteristics, including minimum phasing and bubble energy. The emitted energy varies with both azimuth and take-off angles. To improve designature results on the Mad Dog 3D VSP data, which were long offsets and full azimuth, we applied an inversion-based, shot-to-shot directional designature using near-field hydrophone (NFH) data. NFHs are often installed approximately 1 m above each gun in the gun array to check gun misfires and gun-array separation during acquisition.

We performed shot-to-shot 3D VSP directional designature by iterative inversion in the tau-p domain to find the model that best matched with the data after convolving with the directional source signature. Once the most representative model was obtained, the designatured data was obtained by convolving the predicted model and a zero-phased wavelet free of bubble energy. Figure 4 shows the time-domain seismic and its auto-correlation QC (a) before and (b) after shot-to-shot directional designature. We can clearly see the bubble energy was attenuated effectively. Migrated images in Figure 5 reveal the improved imaging resolution after directional designature was applied.

After all the pre-processing techniques were applied to the Mad Dog 3D VSP data, including the two key pre-processing steps described above, the VSP up-going energy of XYZ components were migrated separately, and then merged together to obtain constructively stacked migrated images. After this optimal stacking of XYZ images, our final VSP image was higher resolution in the target area below the wellbore and more clearly indicated the normal fault in the target area compared to the legacy streamer image (Figure 6).

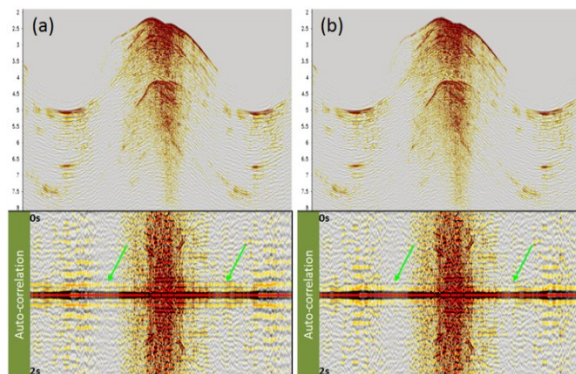


Figure 4: Receiver gather and its corresponding auto-correlation (a) before and (b) after shot-to-shot directional designature. Green arrows indicate how the bubble energy was attenuated effectively after our directional designature algorithm.

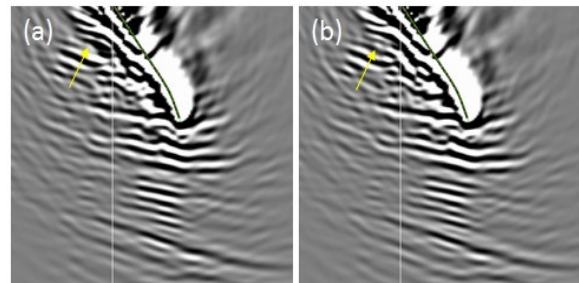


Figure 5: Migrated images (a) before and (b) after shot-to-shot directional designature for 3D VSP data. The yellow arrow indicates an area of the resulting improved resolution.

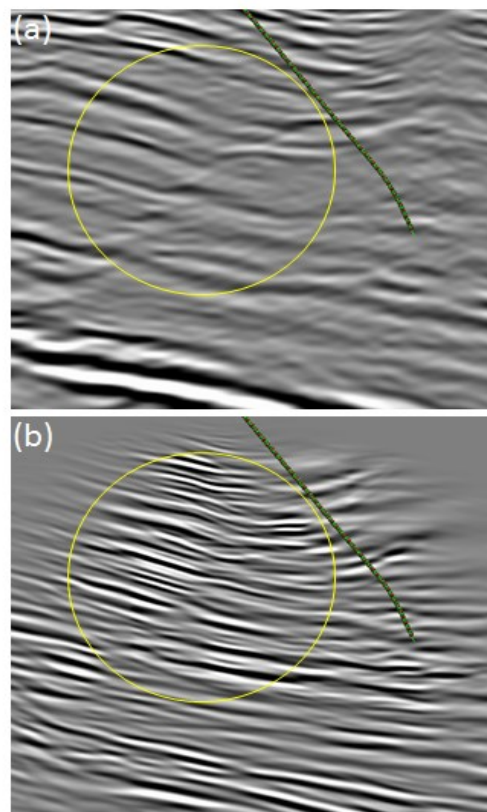


Figure 6: Migrated images of (a) legacy streamer data and (b) 3D VSP data. Red and green dots indicate receiver locations along the wellbore. 3D VSP imaging clearly provides higher resolution and better fault definition in the highlighted circle region.

Multiple migration imaging

To image the local area near wellbores, traditional VSP imaging uses the up-going primary, in which energy propagates downward from the source at the sea surface, reflects from the subsurface, then travels back up to the

3D VSP imaging at Mad Dog, Gulf of Mexico

geophones located in the wellbore, i.e., first order up-going waves. Migration of multiples, on the other hand, utilizes the energy that travels farther up and is reflected back down to the geophones, i.e., first-order down-going waves. This multiple energy recorded in VSP data illuminates a significantly larger area and may therefore expand our imaging capability. The multiple wavefield can illuminate the events lying below or above the geophone array, while the primary reflections only illuminate horizons that lie below the recording geophones. Here, we mainly focus on shallow over-burden imaging using an algorithm for migration of multiples. All the multiple energy are used for the VSP multiple migration imaging. To image the deeper target area with higher confidence using multiple energy, we need to further reduce the crosstalk noise when utilizing the multiple energy. Figure 7 shows a section view of the migration imaging of (a) streamer data, (b) 3D VSP multiple migration, and (c) 3D VSP up-going data. Compared to the 3D VSP up-going imaging, multiple migration imaging illuminates events above receivers and shallow sediment clearly. The VSP multiple migration imaging greatly extended the imaging capability vertically and laterally. However, due to the VSP acquisition geometry, VSP multiple migration imaging may not be able to image true dipping of subsalt events which are far away from the wellbore correctly.

To demonstrate the quality of shallow sediment images by 3D VSP multiple migration, a water bottom horizon map extracted from (a) legacy streamer data and (b) 3D VSP multiple migration are compared in Figure 8. The multiple migration from the 3D VSP survey provided the clear illumination for shallow sediment, which could not be imaged using VSP up-going wavefield alone.

Conclusion and Discussion

3D VSP surveys have the potential to provide high quality seismic images near the wellbore, even in subsalt areas that are challenging to image with streamer data. Unlocking the imaging potential at the Mad Dog field required special consideration and innovative pre-processing techniques. XYZ vector field reorientation using 3D TTI finite-difference modeling was particularly impactful, resulting in better event coherency in the migrated images. Shot-to-shot directional designature utilizing NFH data effectively removed the bubble energy and gun signature. When compared to the streamer data, the 3D VSP final image provided higher resolution and better fault definition near the subsalt target region. To study the potential imaging impact of additional down-going energy, we utilized migration of multiples to expand the VSP imaging both vertically and laterally. The shallow overburden, which could not be imaged by the VSP up-going wavefield alone, was clearly imaged by the VSP multiple energy, albeit with

contamination of multiple crosstalk. Further work may be needed to remove the crosstalk noise in order to improve the imaging of subsalt target events using a multiple migration algorithm.

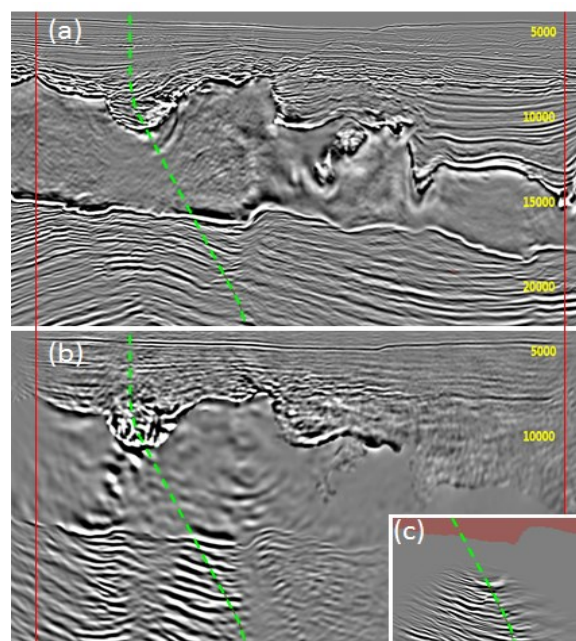


Figure 7: Migrated images of (a) legacy streamer data, (b) 3D VSP data imaged with migration of multiples, and (c) 3D VSP up-going data (red colormap indicates the salt geometry). Vertical red lines indicate shot coverage of the 3D VSP survey and the green dashed line shows the well deviation profile.

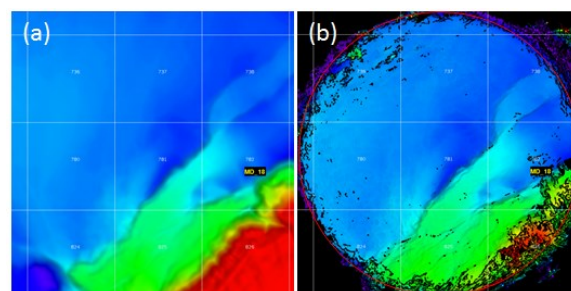


Figure 8: Water bottom profile extracted from (a) legacy streamer migrated image and (b) 3D VSP multiple migration image (red circle indicates the shot coverage for Mad Dog 3D VSP survey).

Acknowledgments

We thank BP, BHP, Chevron and CGG for permission to publish this work. We also thank Timmy Dy and Kawin Nimsaila for their significant contribution and fruitful discussions.

EDITED REFERENCES

Note: This reference list is a copyedited version of the reference list submitted by the author. Reference lists for the 2016 SEG Technical Program Expanded Abstracts have been copyedited so that references provided with the online metadata for each paper will achieve a high degree of linking to cited sources that appear on the Web.

REFERENCES

- Greenhalgh, S. A., and L. M. Mason, 1995, Orientation of a downhole triaxial geophone: *Geophysics*, **60**, 1234–1237, <http://dx.doi.org/10.1190/1.1443852>.
- Lee, C.-C., Y. Li, S. Ray, and G. Poole, 2014, Directional designature using a bootstrap approach: 84th Annual International Meeting, SEG, Expanded Abstracts, 4253–4257, <http://dx.doi.org/10.1190/segam2014-1287.1>.
- Leung, V., M. Wong, and R. Zhang, 2013, Up- and down-going wave multiples RTM imaging for VSP: 83th Annual International Meeting, SEG, Expanded Abstracts, 5052–5056, <http://dx.doi.org/10.1190/segam2013-0631.1>.
- O'Brien, J., B. Farmani, and B. Atkinson, 2013, VSP imaging using free-surface multiples: A case study from the Gulf of Mexico: *The Leading Edge*, **32**, 1258–1266, <http://dx.doi.org/10.1190/tle32101258.1>.
- Rollins, F., W. Gou, S. Ji, Y. Li, P. Ariston, and J. Bowling, 2013, TTI imaging with multi-wide azimuth data — A case study at Mad Dog, GOM: 83rd Annual International meeting, SEG, Expanded Abstracts, 3084–3089, <http://dx.doi.org/10.1190/segam2013-0720.1>.
- Rollins, F., J. R. Sandschaper, Q. Li, F. Ye, and S. Chakraborty, 2015, Calibrating 3D VSP image area with finite difference modeling — A case study in Gulf of Mexico: 85th Annual International Meeting, SEG, Expanded Abstracts, 3517–3521, <http://dx.doi.org/10.1190/segam2015-5873629.1>.
- Xu, L., J. Yang, H. Chen, M. Vu, and P. Wang, 2015, Application of 3D source deghosting and designature to deep-water ocean bottom node data: 85th Annual International meeting, SEG, Expanded Abstracts, 4631–4635, <http://dx.doi.org/10.1190/segam2015-5924634.1>.